Red cells dynamic morphologies govern blood shear thinning under microcirculatory flow conditions

Luca Lanotte [*], Johannes Mauer [†], Simon Mendez [‡], Dmitry A. Fedosov [†], Jean-Marc Fromental [§], Viviana Claveria [*], Franck Nicoud [‡], Gerhard Gompper [‡], and Manouk Abkarian [*]

[*]Centre de Biochimie Structurale, CNRS UMR 5048 - INSERM UMR 1054, University of Montpellier,34090 France,[†]Institute of Complex Systems and Institute for Advanced Simulation, Forschungszentrum Jülich, 52425 Germany,[‡]IMAG UMR 5149 CC 051, University of Montpellier, 34095 Montpellier, France, and [§]Laboratoire Charles Coulomb, CNRS UMR 5587, University of Montpellier,34095 France

Submitted to Proceedings of the National Academy of Sciences of the United States of America

Blood viscosity decreases with shear stress, a property essential for an efficient perfusion of the vascular tree. Shear-thinning is intimately related to the dynamics and mutual interactions of red blood cells (RBCs), the major component of blood. Because of the lack of knowledge about their behavior under physiological conditions, the link between RBCs dynamics and blood rheology remains still unsettled. Performing experiments and simulations in microcirculatory flow conditions of viscosity, shear rates and volume fractions, our study reveals new RBCs dynamics, which govern shear-thinning. In contrast to the current paradigm, which assumes that RBCs align steadily around flow direction while their membrane and cytoplasm circulate, we show instead that RBCs successively tumble, roll, deform into rolling stomatocytes, and finally adopt highly-deformed poly-lobed shapes for increasing shear stresses, even for semi-dilute volume fractions of the microcirculation. Our results suggest that any pathological change in plasma composition, RBCs cytosol viscosity, or membrane mechanical properties will impact the onset of these morphological transitions, and should play a central role in pathological blood rheology and flow behavior.

blood rheology | red blood cell | cell dynamics | blood simulation

Significance statement. Our work reveals new RBCs dynamic morphologies which govern blood shear-thinning under microcirculatory flow conditions, contrary to the current paradigm assuming steady RBCs orientation and membrane circulation. Our results suggest that any pathological change in RBCs local rheology will impact the onset of these morphological transitions and should play a key role in pathological blood flow.

Red blood cells (RBCs) are the main cellular component of whole blood (WB). About a thousand times more concentrated than white blood cells and platelets, the volume fraction of RBCs or their hematocrit (Ht) is as high as 45%. Local dynamics and interactions of RBCs govern blood rheology and control proper perfusion of the entire vascular tree. In particular, WB exhibits a strong shear-thinning behavior in shear flow [1, 2] which is determined by the aggregability and deformability of RBCs [3], since the suspending plasma behaves essentially as a Newtonian fluid with a constant shear viscosity of about 1.2 cP at 37°C [1, 4]. Macromolecules dispersed in the plasma, such as fibrinogen, induce an attractive force between RBCs leading to their aggregation [5]. Because RBCs have a biconcave disk-like shape at rest, they form long floppy rouleaux structures which can reversibly and continuously break down to single flowing discocytes for increasing shear rates up to tens of s^{-1} [6, 7]. This change in microstructure is indeed accompanied by a strong viscosity drop from ~ 100 cP down to about ~ 10 cP [3]. However, for shear rates between 10 and 1500 s^{-1}, which are common in the microcirculation [8, 9], only the deformability and dynamics of RBCs can account for a further four-fold decrease in WB viscosity down to values as low as $2-3$ cP [3]. This value strongly depends on the hematocrit and the viscosity of RBCs hemoglobin cytoplasm, which is around 5 cP at 37°C [10].

The link between cellular deformability and shear-thinning remains unsettled, even though it is crucial in understanding blood flow both in health and disease: altered RBCs deformability [11] are correlated with impaired perfusion, increase in blood viscosity, and vaso-occlusion in microcirculatory disorders such as diabetus mellitus, or hemoglobinopathies like sickle cell anemia. Observations of RBCs dynamics in microtubes [12] and rheoscopes [13], realized during the 1970s and 1980s, have led to the foundation of the current paradigm for shear-thinning, comforting an emulsion analogy for blood rheology inherited from the 1960s [1, 2]. While at low shear stresses (less than about 0.05 Pa) single RBCs flip like a coin, they reach a steady orientation for increasing flow strength [13, 14] allowed by a tank-tread-like circulation of their membrane [13]. Such droplet-like behavior should effectively assist the flow by minimizing disturbances to streamlines and has been successfully used to deduce some mechanical properties of RBCs membrane in dilute conditions [15, 16]. However, steady tank-treading occurs only when RBCs are dispersed into a viscous aqueous solution (often of dextran polysaccharides), which is several times more viscous than the inner cytoplasm. Such a viscous environment around single cells is supposed to mimic the effective high-shear-rate viscosity of the crowded conditions present in WB [17]. Therefore, shear-thinning paradigm is rooted in RBCs ability to tank-tread whatever the hematocrit in response to high shear stresses [7].

Recent experiments realized on dilute RBC suspensions with outer viscosities similar to that of the hemoglobin-rich cytoplasm, have demonstrated however that the solid-like tumbling motion is not replaced by tank-treading for increasing shear rates, but rather by a typical solid rolling motion, where the axis of symmetry of the discocyte lies in the direction of vorticity [18]. Even for shear stresses up to 0.5 Pa, no fluidization of the membrane was observed, demonstrating the important role the inner-to-outer viscosity ratio λ plays on local dynamics. In fact, plasma viscosity under physiological conditions is about five times smaller than that of RBCs cytosol. New

Reserved for Publication Footnotes

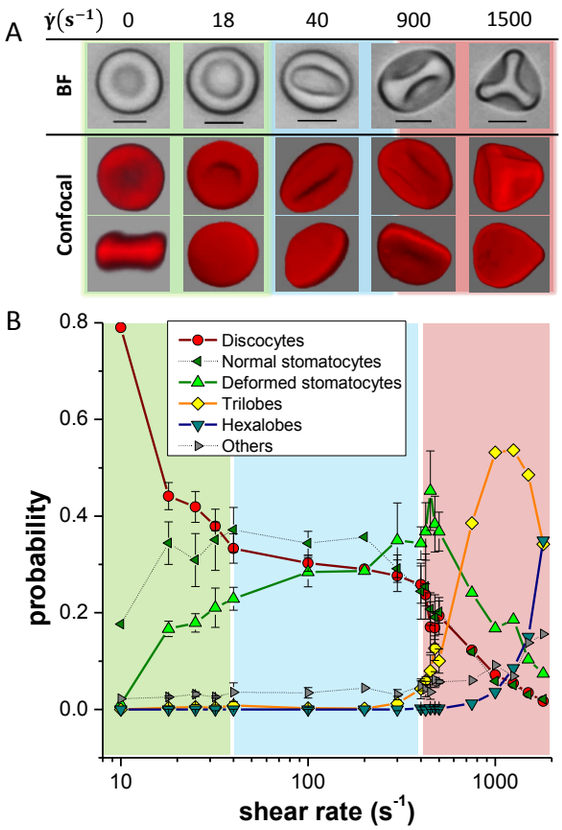

Fig. 1. Investigation of RBC shapes at different shear rates in a cone-and-plate rheometer. A) Observation of hardened cells by optical (black and white) and confocal (red) microscopy: with increasing $\dot{\gamma}$ the formation of highly deformed stomatocytes and then polylobed cells (trilobe and hexalobe) are detected (scale bars are 5 μm). B) Shape distribution of RBCs populations in samples hardened at different shear rates: the three regions in color highlight different regime of decrease of discocytes population. The error bars represent triplicate measurements realized in the two rapidly varying regions. They illustrate the typical variance of the measurements.

studies are thus required to investigate RBCs local dynamics at such low viscosity conditions and high shear rates.

In this work, we explore the shape and dynamics of RBCs in the range of shear rates $\dot{\gamma}$ between 10 to 1500 s^{-1} and hematocrits between 15 up to 45% relevant for the microcirculation [8, 9]. We correlate RBCs dynamic morphologies with blood shear-thinning measured by rheometry. Using microfluidics, we demonstrate that RBCs show unexpected movement characterized by rotating polylobed shapes, with no clear tank-treading of their membrane. Experimental results are corroborated by two different 3D simulation techniques: a continuum approach [19] based on the finite-volume method and a mesoscopic approach [20] based on the smoothed dissipative particle dynamics (SDPD) method [21]. We discuss the implication of this work for microcirculatory flow and re-interpret the classical shear-thinning conjecture.

Results

Morphology of RBCs in simple shear flow. We first explore the morphologies of single RBCs at 37°C subjected to a simple shear flow in a range of $\dot{\gamma}$ between 10 s^{-1} and 2000 s^{-1} using a cone-and-plate rheometer. Cells are quickly hardened with an aldehyde treatment while flowing (see protocol in Materials and Methods). Samples of these hardened RBCs (HRBCs) are then withdrawn from the plate of the rheometer and visualized by bright field (BF) and confocal microscopy after fluorescent dying of their membranes. Typical images of the fixed shapes are shown in Fig. 1A for a given sample. We classify the different morphologies of HRBCs as a function of $\dot{\gamma}$ in Fig. 1B using an in-house image-analysis program.

RBCs subjected to weak shear rates (< 10 s^{-1}) commonly keep their biconcavity similar to typical discocytes at rest (Fig. 1A). For $\dot{\gamma}$ increasing from 10 to 40 s^{-1} however, the percentage of discocytes decreases more than twice (Fig. 1B). This is due to the systematic development of two populations of cup-shaped stomatocytes: one with a circular rim and another with an elliptical one with an aspect ratio smaller than 0.95. Examples of these deformed stomatocytes are displayed in Fig. 1A at 18 and 40 s^{-1}, respectively. At $\dot{\gamma} = 45$ s^{-1}, the fraction of discocytes has dramatically dropped to about 30% of the population, while the total amount of stomatocytes has jumped nearly to 65%. These values remain nearly constant for both cell populations up to about 400 s^{-1} (light blue color region of Fig. 1A). However, in the region between 45 s^{-1} and 400 s^{-1}, the fraction of circular-rim-shaped stomatocytes decreases, and gets replaced by the population of elliptical-rim-shaped stomatocytes with an increased ellipticity.

At $\dot{\gamma} \approx 400$ s^{-1}, a new transition takes place. We observe a sharp increase in the population of deformed stomatocytes which appear to be strongly folded (around 475 s^{-1} in Fig. 1B). Most importantly, we also see the rise of a new population of RBCs showing large lobes on their surface. In most cases, we find cells with three or six lobes forming tetrahedron, which will be henceforth referred to as trilobes or hexalobes, respectively. In the region 400 $s^{-1} < \dot{\gamma} < 2000$ s^{-1}, marked by a light red color in Fig. 1B, we observe the nearly disappearance of discocytes (less than 10%) and the formation of trilobes and to a lesser degree hexalobes, such that the polylobed RBCs represent almost 70% of the sheared population at the highest shear rates. Moreover, rapid rise of hexalobe population is found for $\dot{\gamma} \sim 2000$ s^{-1}, suggesting a direct correlation between the number of lobes and shear strength.

RBCs dynamics in flow. To understand further how the acquired morphologies couple to flow and to rule out hardening artifacts, we perform complementary microfluidic experiments with high-speed video microscopy at 25°C using dilute suspensions of RBCs ($Ht \approx 1\%$) in PBS/BSA (no hardening). The suspension is fed at increasing flow rates into a circular microcapillary for the same range of shear rates explored by rheometry. Local shear rate is evaluated by measuring both the local cell velocity and distance from the capillary walls. Different dynamics are detected for increasing values of this estimated $\dot{\gamma}$. The time sequences shown in Fig. 2A, are obtained in a field of view of about 300 μm long. At low shear rates ($\dot{\gamma} < 40$ s^{-1}), the tumbling-to-rolling transition is observed, where the axis of symmetry of discocytes gradually aligns with the vorticity direction. As in the rheological setup, the number of rolling RBCs becomes significant for increasing shear rates. In addition, a substantial increase in the population of cup-shaped stomatocytes is clearly detected, which show a rolling motion in the flow as illustrated in Fig. 2A at $\dot{\gamma} = 150$ s^{-1}. Moreover, observations reveal both tumbling and vacillating-breathing behaviors (see Movie S1) of folded stomatocytes (Fig. 2A, blue box) with the latter being largely detected at high shear strengths $\dot{\gamma} > 350$ s^{-1} (see examples in Fig. 2 for 250 $s^{-1}$and 500 s^{-1}). Furthermore, these *in vitro* investigations confirm the formation and stability of polylobed shapes at higher shear rates. Two trilobes are depicted in side and top views at 750 and 800 s^{-1}, respectively, in Fig.

2A (light red color box) and Movie S2. At such high shear rates, RBCs elongate in the vorticity direction, and display three lobes which rotate around the center of mass. An even more solid-like rotation is observed for hexalobes under comparable flow conditions (last time sequence in Fig. 2A and Movie S3). These experiments show that no sharp morphological transition occurs for increasing shear rates, but rather a marked variation in shape distribution of RBC populations is present. Finally, thanks to our pressure injection system, we can produce very fast "stop flow" experiments. These experiments nicely demonstrate the dynamical nature of polylobed morphologies, since either trilobes or hexalobes return rapidly to their resting discocyte shape, when the flow is stopped, as depicted in Fig. 2B and Movie S4. Noteworthy, the population of stomatocytes keeps its shape longer and relaxes to the discocyte population on a longer time scale of tens of minutes.

To complement the experiments, we also perform numerical simulations of isolated RBCs in simple shear flow for varying shear rates, using both SDPD and YALES2BIO softwares (see Materials and Methods). The simulated dynamics is presented in Fig. 2A using only YALES2BIO results, since agreement between the two simulations is very good. Simulations confirm the sequence of shapes and dynamics observed experimentally as well as their dependence on $\dot{\gamma}$ as shown in Fig. 2A and Movies S5 and S6. In comparison to experiments, simulations provide a detailed information about dynamic behavior of RBCs in flow. For example, the same cell may have different stable shapes under flow (observed during several hundreds of time units $1/\dot{\gamma}$) depending on its initial orientation with respect to the flow. In particular, stomatocytes can display both rolling-like or tumbling-like motion; rolling deformed stomatocytes (see Movie S5) and tumbling trilobes (see Movie S6) might be found for similar shear rates. However, the sequence of shapes found experimentally appears to be qualitatively robust to moderate changes in the RBC mechanical properties, which has been tested in simulations. One difference between experimental and simulation results is hexalobed deformation of RBCs (Fig. 2A at the bottom), which has been observed in simulations only as a transient state. Nevertheless, in none of the simulations performed for the range $1\ \mathrm{s}^{-1} < \dot{\gamma} < 2000\ \mathrm{s}^{-1}$ a tank-treading ellipsoidal RBC has been obtained.

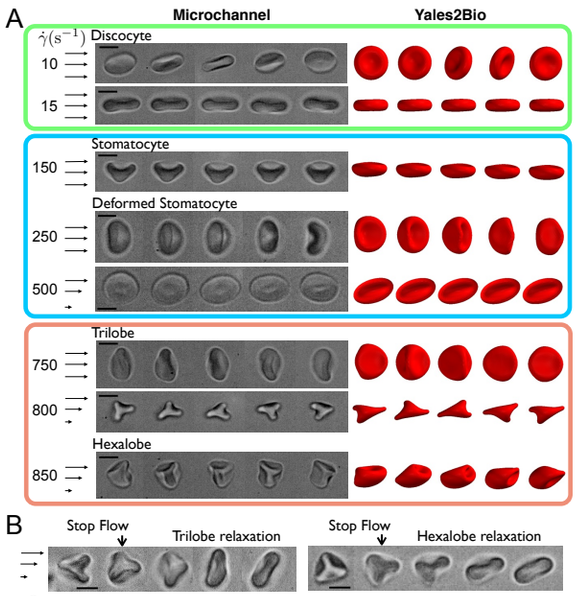

Fig. 2. Microfluidic observations of RBC dynamics in shear flow. A) Sequence of RBC deformations at various $\dot{\gamma}$: time lapse = 20 ms ($\dot{\gamma} = 10\ \mathrm{s}^{-1}$), 6 ms ($\dot{\gamma} = 15\ \mathrm{s}^{-1}$), 3.25 ms ($\dot{\gamma} = 150, 250$, and $500\ \mathrm{s}^{-1}$), 0.6 ms ($\dot{\gamma} = 750\ \mathrm{s}^{-1}$), 1.75 ms ($\dot{\gamma} = 800\ \mathrm{s}^{-1}$), and 0.6 ms ($\dot{\gamma} = 850\ \mathrm{s}^{-1}$). Right panel shows analogous time sequences of RBCs obtained with YALES2BIO simulations: time lapses are given in $1/\dot{\gamma}$ units from top to bottom: 8, 7, 6, 6, and 7 for the four last cases. B) Stop flow sequences of (left) a trilobe with a relaxation time of 1 s and intermediate images separated by 0.23 and 0.56 s, (right) a hexalobe with relaxation of 1.2 s and successive images with a time interval of 0.32 and 0.71 s. Scale bars are 5 μm.

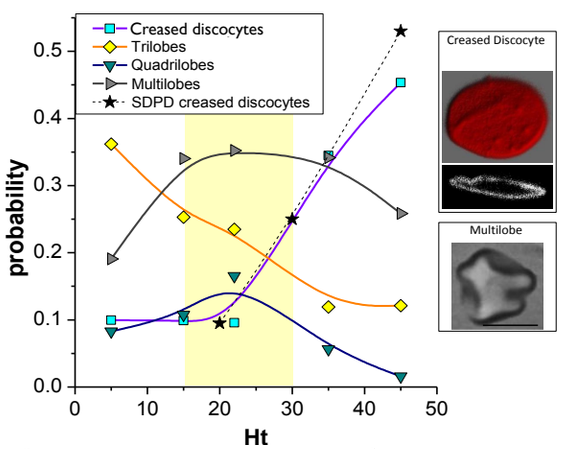

Fig. 3. Shape distributions of HRBCs at 900 s^{-1} in suspensions with different Ht. For clarity, discocytes and stomatocytes number densities have been omitted since they are negligible. Inset: black frames on the right, a top view and a cross section of a creased discocyte acquired by confocal microscopy as well as an image of a multilobe in BF (scale bar is 5 μm). Physiological hematocrits are indicated by the light yellow region.

Morphology and dynamics of RBCs at high hematocrits. To evaluate the prevalence of polylobed shapes at physiologically relevant shear rates and hematocrits, similar hardening experiments were realized for several RBC suspensions with different Ht values of 5, 15, 22, 35 and 45%. $\dot{\gamma} = 900\ \mathrm{s}^{-1}$ (at 37°C) has been selected for these experiments, since the analysis for dilute suspensions in Fig. 1B has shown a maximum in the population of trilobes at this shear rate. Figure 3 indicates a significant decrease in the probability to obtain polylobed HRBCs for increasing Ht. The percentage of trilobes and hexalobes, which amounts for about 55% of the entire population at $Ht = 5\%$, is more than halved when the hematocrit reaches 45%. In addition, at high enough Ht many HRBCs display a deformed shape with multiple irregular lobes, making it difficult to precisely classify their morphology; these cells will be called "multilobes" with an illustration in the lower inset of Fig. 3. The fraction of these multilobed RBCs seems to be rather stable amounting for $25\% - 35\%$ of the total population. However, the onset of a new cell morphology is detected for increasing Ht. Flattened discocytes characterized by one or several grooves or creases on their membrane have been found and are illustrated in the inset of Fig. 3 by optical and confocal microscopy. The fraction of creased discocytes increases significantly at high Ht values amounting for almost 50% of the sample at $Ht = 45\%$. In contrast to the vast majority of polylobed RBCs in dilute suspensions, the formation of flat cells with creases is a clear effect of mutual hydrodynamic interactions between cells in such dense suspensions. Indeed, the total percentage of lobed cells with increasing Ht has the exact inverse evolution of that for creased discocytes as shown in Fig.3. Interestingly, physiological hematocrits in the microcirculation lie in the range $15 - 30\%$ (light yellow region in Fig.3),

in which a clear coexistence of different cell morphologies with a domination of lobed shapes is present.

To corroborate the existence of such folded and irregular structures in flow at high Ht, we have performed SDPD simulations with dense RBCs suspensions. The analysis of creased-discocyte population for different Ht is presented in Fig. 3 along with the corresponding experimental data showing a good qualitative agreement. Figure S1 also shows RBC-extension distributions for different Ht values, which are averaged over multiple RBCs and many time instances (a typical simulation is shown in Movie S7). The extension distributions clearly show that RBCs become more stretched in the flow as Ht is increased and that at low enough Ht polylobed shapes dominate, while at $Ht = 45\%$ the fraction of creased discocytes becomes larger than one half. The coexistence of various cell morphologies and the evolution of different RBCs populations with increasing Ht are consistent with the observations made experimentally.

The role of cell deformability in shear-thinning rheograms. Now, we re-examine the interpretation of classical shear-thinning rheograms for human blood, which were introduced in the 1970s [3] and provided the seminal link between shear-induced RBC deformation, tank-treading, and shear-thinning. We perform experiments at $Ht = 45\%$ suspending RBCs in either PBS/BSA or their native plasma. The samples are sheared in the rheometer at 37°C (using both Couette and cone-and-plate geometry) for the range of $\dot{\gamma}$ between 5 s^{-1} and 2000 s^{-1}. The relative viscosity (η_{rel}), defined as the ratio between the measured viscosity of the suspension (η_s) and the viscosity of the suspending medium (η_m), is obtained for different $\dot{\gamma}$. Consistently with previous works [3], at low shear rates, washed blood has a significantly lower viscosity than WB since plasma induces aggregation. From $\dot{\gamma} \approx 10$ s^{-1}, viscosity curves for both washed blood and WB merge into a common shear-thinning behavior as shown in Fig. 4A. To understand the role of shape change in this regime, we compare washed blood rheology with that of two HRBC suspensions at 45% Ht: one with stiff discocytes hardened at rest and the other one with polylobed cells obtained by hardening cells previously in the rheometer at $\dot{\gamma} = 1500$ s^{-1} and re-suspending them in PBS/BSA at the desired 45% Ht. Both suspensions of HRBCs show a nearly Newtonian behavior except for shear rates above 400 s^{-1} where the onset of a slight shear-thickening is observed especially for hardened discocytes. This behavior is similar to shear-thickening reported for rigid colloidal suspensions [22, 23]. For both HRBC dispersions viscosity values are larger than those for washed blood; however, the sample with hardened polylobes yields a 70% lower relative viscosity than that for stiffened discocytes, as seen in Fig 4A. These results indicate that from $\dot{\gamma} = 10$ s^{-1} up to a few hundred s^{-1}, shear-thinning is largely determined by the change in RBC dynamics from tumbling to rolling and by the deformation of RBCs into elongated stomatocytes. Beyond $\dot{\gamma} \sim 400$ s^{-1} however, a further viscosity drop is related to the formation of polylobed and flattened shapes discussed above.

SDPD simulations performed for $\lambda = 5$ and $Ht = 45\%$ quantitatively capture shear-thinning as shown in Fig. 4A. A closer look at RBCs shapes for different shear rates essentially confirms experimental observations. For moderate shear rates up to a few hundred s^{-1}, a prevalence of stomatocytes and multilobe cells is found, while at high shear rates, flattened RBCs are mainly observed. Stomatocytes and polylobes found for moderate $\dot{\gamma}$ values show a tumbling-like dynamics. The dynamics of flattened RBCs at high shear rates resembles a tank-treading motion; however, these cells display persistent and dynamic membrane deformations represented by small creases or larger lobes, which continuously form and disappear. Tank-treading with a steady ellipsoidal shape was never observed in simulations and the motion of flattened RBCs at high shear rates is likely to be a superposition of both cell stretching and lobes rotation.

Finally, to highlight the importance of λ for the presence of lobular shapes and their role in shear-thinning in comparison to steady tank-treading, we perform rheological measurements for suspensions of normal RBCs dispersed in solutions with increasing viscosities modulated by various dextran concentrations of 2%, 4% and 9% (wt/wt) in PBS (respective viscosities: 3.4, 10.2 and 38.8 mPa.s). Hematocrit is kept at 45% and the suspensions are sheared at 25°C for the range of $\dot{\gamma}$ between 10 s^{-1} and 2000 s^{-1} (without hardening). Figure 4B presents relative viscosities of these suspensions as a function of the shear stress τ ($= \eta_s \dot{\gamma}$). The curves for PBS/BSA and 9% dextran solution display inconsistent trends. In PBS/BSA, which corresponds to high viscosity ratios ($\lambda \approx 10$ at 25°C), a significant and continuous decrease of η_{rel} is observed for increasing τ up to the rheometer limit of about 6 Pa. In contrast, 9% dextran suspensions ($\lambda \approx 0.25$) exhibit a slight shear-thinning for stresses close to 1 Pa, but η_{rel} yields a plateau for higher

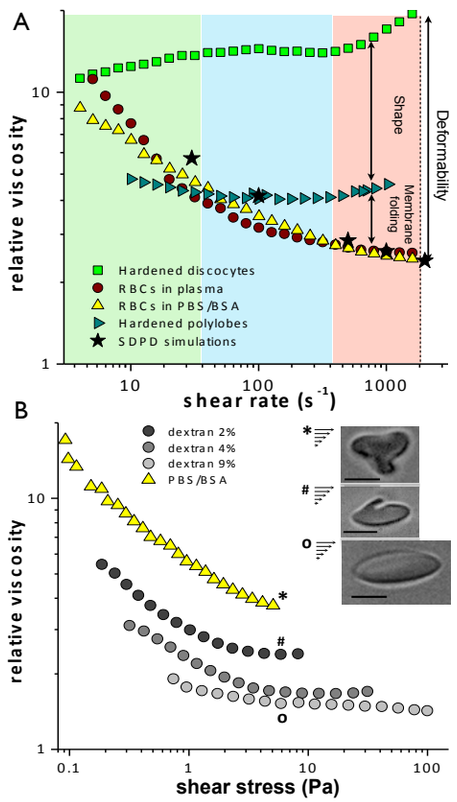

Fig. 4. Rheology of dense suspensions of RBCs ($Ht = 45\%$). A) Relative viscosity of the suspensions of deformable RBCs in plasma (red) and in PBS/BSA (yellow) as a function of $\dot{\gamma}$ in comparison to the suspensions of washed cells hardened at rest (green) and at $\dot{\gamma}$=1500 s^{-1} (blue). Suspensions of deformable RBCs show a typical shear-thinning for increasing $\dot{\gamma}$, whereas hardened samples have a nearly Newtonian behavior. SDPD simulation data (black stars) are also shown for deformable cells and agree well with the experimental results for RBCs suspended in plasma or in PBS/BSA. B) Rheology of washed blood in comparison to the suspensions of RBCs in solutions with different dextran concentrations (T=25 °C). The effect of viscosity ratio λ is highlighted in the inset by the illustration of single cells flowing in both PBS/BSA and dextran solutions in microfluidics at a comparable shear stress τ. The scale bars are equal to 5 μm.

stresses (see Fig. 4B). Samples with 2% and 4% dextran solutions show an intermediate behavior, in which the occurrence of an increasingly significant shear-thinning for increasing λ is detected. In parallel, we have performed microfluidic observations of single RBCs flowing in 2% and 9% dextran solutions at $Ht = 1\%$ for comparable shear stresses. Contrary to the behavior of RBCs in PBS/BSA, cells in 9% dextran solutions do not assume polylobed shapes, but show a rather sharp transition from rigid tumbling discocytes to tank-treading ellipsoids which elongate with increasing stresses. This transition takes place at $\tau \sim 1Pa$ which is consistent with the change in slope of the corresponding η_{rel} curve in Fig. 4B. In the inset of Fig. 4B an illustration of the effect of λ on RBC dynamics is presented. Images show the shapes of cells dispersed respectively in PBS/BSA, 2% and 9% dextran solutions and flowing in a microchannel with the same estimated local shear stress of $\tau = 6$ Pa. A decrease in λ promotes in-flow orientation, elongation and simultaneous reduction of lobes size (see Movie S8). When $\lambda \approx 0.25$, polylobed cells are completely replaced by elongated tank-treading ellipsoids (see inset in Fig. 4B). Noteworthy, all images in the inset of Fig. 4B and movies in *Supporting Information* refer to RBCs flowing in microchannels in which the presence of a gradient in $\dot{\gamma}$ can potentially affect RBCs dynamics, while rheological measurements were performed under pure shear flow conditions. However, comparison between off-center shape sequences in 50 μm capillaries and simple-shear YALES2BIO simulations presented in Fig. 2A indicates a rather marginal effect of the gradient of shear rate.

Discussion

Without aggregation, blood continuous shear-thinning is the result of a rich dynamical behavior of RBCs population, based primarily on the inability of RBCs to tank-tread under physiological conditions ($\lambda \approx 5$). In this study, we have observed a diversity of shapes and dynamical states of RBCs for increasing shear rates and the development of a large fraction of highly deformed and polylobed cells for $\dot{\gamma} > 400$ s^{-1} (Figs. 1 and 2) which has been confirmed by simulations.

For single cells in dilute suspensions, and for $\dot{\gamma} < 1$ s^{-1}, the biconcave shape is preserved and RBCs behave like rigid oblate ellipsoids, such that the membrane and the enclosed fluid rotate as a rigid body. For increasing shear rates up to 10 s^{-1}, more and more cells are found to roll on their edge as previously observed in experiments using rheoscopes [24] and more recently in flow chambers [25, 18]. Shear-thinning in this range of shear rates is therefore mainly controlled by discocyte orientation. Rolling has its origin in shear elasticity of the membrane. Under physiological conditions, membrane tank-treading is forbidden due to the relatively high internal viscosity as predicted by viscous ellipsoidal models of the RBC [26]. However, during each tumbling period the membrane elements oscillate around a given position and this local oscillatory strain seems to destabilize RBCs from tumbling toward rolling [27] instead of tank-treading. Though not fully settled, this phenomenon is well captured by our simulations and is described as a stable motion in several recent numerical simulations of capsules [28] and RBCs [29].

In the range of shear rates between 45 and 400 s^{-1}, a large population of the rolling discocytes looses one dimple and becomes rolling stomatocytes displaying at first more frequently a circular rim up to 45 s^{-1} and then a breathing elliptical rim for shear rates reaching 400 s^{-1}. In this second morphological transition, rolling stomatocytes are showing a smaller cross-section to shear flow than rolling discocytes, reducing their disturbances of the streamlines. This leads to a further shear-thinning. Both our numerical approaches capture this flow-induced morphological transition for single RBCs. The loss of the dimple happens abruptly in simulations highlighting a buckling instability, which is also confirmed experimentally by the long time scales (minutes) necessary for the population of stomatocytes to relax to a discocyte shape.

Beyond 400 s^{-1}, the dilute population of RBCs is subjected to a new shift in morphology and large lobes develop on the surface of the cells (Fig. 1A). These out-of-plane deformations are again a signature for a lack of fluidization of the membrane even for the largest stress of 6 Pa we were able to reach both experimentally (with the rheometer and in microflows) and numerically. Noteworthy, Sutera and Mehrjardi [30] studied in the 1970s the morphology of cells hardened in PBS solutions at very high shear stresses ($\tau \geq 10$ Pa). Their images at $\tau = 10$ Pa show the presence of pronounced concavities on RBCs similar to those we observe for polylobed cells. Our experiments confirm how lobes are directly associated with a large enough viscosity contrast λ since they vanish in very viscous dextran solutions as shown in Fig. 4 (from $\lambda \approx 2.9$). However, the exact nature of these transitions and the development of folded shapes remain to be understood. Modifications of a RBC membrane at rest can also induce similar transformations observed here for increasing shear rates. Theoretically, a large equilibrium-shape variety has been obtained for RBCs including stomatocytes, with circular and deformed rims, and trilobes (named knizocytes in the literature), by changing the resting elastic state of the cytoskeleton and the area difference between lipid leaflets in the model [31]. Despite this striking similarity, the dynamic shapes in our simulations have been observed without any explicit modification of the membrane. These results open the road for further experimental investigations on the possible flow-induced modifications of RBCs membrane and their impact on dynamics.

Our dilute single-cell experiments and simulations show how out-of-plane deformations are inevitable for increasing shear rates. However, for more concentrated suspensions, a large population of creased and flattened discocytes appears both in experiments (see Movie S9) and simulations (see Movie S7 and Fig. S1). While it is perfectly conceivable that large lobes cannot easily develop on membranes in crowded suspensions, the complex flow between cells seems to counter-balance the inherent tendency of RBCs to elongate more in the vorticity direction. It is this fine balance between vorticity- and flow-direction elongations that aligns cells on average parallel to the flow. Nevertheless, any variations in relative positions between the cells or any collisions immediately give birth to local bulges on the membranes and produce large fluctuations of shapes as seen in RBCs extension distributions (Movie S7 and Fig. S1).

In summary, blood shear-thinning is related to a rich behavior of RBCs in shear flow convoluted with a large distribution of cell shapes for any given flow condition. The lack of membrane fluidity for high viscosity contrast is the key feature which controls RBCs behavior. Besides shear-thinning, several fundamental physiological phenomena have been analyzed under the assumption of membrane tank-treading, such as vaso-regulatory ATP release by RBCs in strong shear flows [32] or the formation of a few-micron thick cell-free layer adjacent to the vessels walls which is responsible for the apparent viscosity drop with decreasing vessel diameter, the so-called Fåhræus-Lindqvist effect [33]. Our study questions the relevance of such droplet-like analogy for RBC dynamics to explain these phenomena and asks to re-explore them both experimentally and theoretically for physiologically relevant viscosity and stress conditions. Finally, our study suggests that in pathological states inducing a change in blood features such

as plasma composition, RBCs cytosol viscosity or membrane mechanical properties, the onset of shape transitions will be impacted and this should play a central role in pathological blood rheology and flow.

Materials and Methods

Blood samples. Fresh venous-blood samples were obtained from healthy consenting donors, thanks to the agreement with a local blood bank to use transfusion bags (EFS, Montpellier) and its components for non-therapeutic purposes. Samples preparation and characteristics are given in *Supporting Information* as well as experiments with then, summarized in Table S1.

Rheology and imaging. Rheology experiments were performed in cone-plate and Couette geometries with a stress-imposed rheometer (AR 2000 - TA Instrument). at constant temperature. Dilute and semi-dilute cells suspensions were rigidified in flow by adding a high glutaraldehyde concentration solution in small volume during flow. Such an amount of glutaraldehyde produces a very rapid, strong and permanent solidification. Both shearing and hardening were carried out within 2 min. Samples were then collected, washed, and suspended in PBS solution for microscopic examination realized both in BF and with confocal microscopy. See details in *Supporting Information*.

Microfluidics and imaging. Microflow observations were realized at 25°C in glass round capillaries with a diameter of 50 μm. Flow rates were adjusted by a OB1 Pressure Controller (ElveFlow) operating up to 2 bar. Images were acquired at a high magnification (60x and 100x objectives) on a Nikon inverted microscope equipped with a high-speed camera Phantom Miro M320S (Vision Research) and subsequently analyzed by a custom image analysis software (ImageJ). See details in *Supporting Information*.

Numerical simulations. Two different in-house softwares were used for numerical simulations. The first one, YALES2BIO [19, 34], is a finite-volume parallel solver for the incompressible Navier-Stokes equations on unstructured meshes. Fluid-structure coupling was implemented using an immersed boundary method adapted to unstructured grids [19]. The second one, the smoothed dissipative particle dynamics method [21], is a mesoscale hydrodynamic particle-based approach which represents fluid flow, while a RBC membrane is modeled as a triangulated network of springs [20], whose vertices are coupled to the fluid via frictional forces [20]. Further details about the numerical methods and setups can be found in *Supporting Information*.

ACKNOWLEDGMENTS. M.A., S.M., F.N. and L.L. acknowledge the support of the OSEO-BPI project Dat@Diag. M.A. and L.L. are grateful for the support from the Labex Numev (convention No. ANR-10-LABX-20). S.M. and F.N. acknowledge the support of the ANR (ANR-11-JS09-0011) and thank Dr. Moureau and Dr. Lartigue (CORIA, UMR 6614) and the SUCCESS scientific group for providing the YALES2 code, which served as a basis for the development of YALES2BIO. Simulations with YALES2BIO were performed using HPC resources from GENCI-CINES (Grant 2015-c2015037194). D.A.F. acknowledges funding by the Alexander von Humboldt Foundation. SDPD simulations were performed using a CPU time allocation at the Jülich Supercomputing Center.

1. Wells RE, Merrill EW (1961) Shear rate dependence of the viscosity of whole blood and plasma. Science 133:763–764.
2. Dintenfass L (1968) Internal viscosity of the red cell and a blood viscosity equation. Nature 219:956–958.
3. Chien S (1970) Shear dependence of effective cell volume as a determinant of blood viscosity. Science 168:977–979.
4. Brust M, et al. (2013) Rheology of human blood plasma: viscoelastic versus Newtonian behavior. Phys. Rev. Lett. 110:078305.
5. Merrill EW, Gilliland ER, Lee TS, Salzman EW (1966) Blood rheology: effect of fibrinogen deduced by addition. Circ. Res. 18:437–446.
6. Qin Z, Durand LG, Allard L, Cloutier G (1998) Effects of a sudden flow reduction on red blood cell rouleau formation and orientation using RF backscattered power. Ultrasound Med. Biol. 24:503–511.
7. Fedosov DA, Pan W, Caswell B, Gompper G, Karniadakis GE (2011) Predicting human blood viscosity in silico. Proc. Natl. Acad. Sci. USA 108:11772–11777.
8. Lipowsky HH (2005) Microvascular rheology and hemodynamics. Microcirculation 12:5.
9. Popel AS, Johnson PC (2005) Microcirculation and hemorheology. Annu. Rev. Fluid. Mech. 37:43–69.
10. Wells R, Schmid-Schönbein H (1969) Red cell deformation and fluidity of concentrated cell suspensions. J. Appl. Physiol. 27:213–217.
11. Diez-Silva M, Dao M, Han J, Lim CT, Suresh S (2010) Shape and biomechanical characteristics of human red blood cells in health and disease. MRS Bulletin 35:382.
12. Goldsmith HL, Marlow J (1972) Flow behaviour of erythrocytes. I. Rotation and deformation in dilute suspensions. Proc. R. Soc. Lond. B 182:351–384.
13. Fischer TM, Stöhr-Lissen M, Schmid-Schönbein H (1978) The red cell as a fluid droplet: tank tread-like motion of the human erythrocyte membrane in shear flow. Science 202:894–896.
14. Abkarian M, Faivre M, Viallat A (2007) Swinging of red blood cells under shear flow. Phys. Rev. Lett. 98:188302.
15. Sutera SP, Pierre P, Zahalak G (1989) Deduction of intrinsic mechanical properties of the erythrocyte membrane from observations of tank-treading in the rheoscope. Biorheology. 26:177–197.
16. Korin N, Bransky A, Dinnar U (2007) Theoretical model and experimental study of red blood cell (RBC) deformation in microchannels. J. BioMech. 40:2088–2095.
17. Fischer TM (1977) Tank tread motion of red-cell membranes in viscometric flow-behavior of intracellular and extracellular markers (with film) (Blood Cells) Vol. 3.
18. Dupire J, Socol M, Viallat A (2012) Full dynamics of a red blood cell in shear flow. Proc. Natl. Acad. Sci. USA 109:20808–20813.
19. Mendez S, Gibaud E, Nicoud F (2014) An unstructured solver for simulations of deformable particles in flows at arbitrary Reynolds numbers. J. Comp. Phys. 256:465.
20. Fedosov DA, Caswell B, Karniadakis GE (2010) A multiscale red blood cell model with accurate mechanics, rheology, and dynamics. Biophys. J. 98:2215–2225.
21. Müller K, Fedosov DA, Gompper G (2015) Smoothed dissipative particle dynamics with angular momentum conservation. J. Comp. Phys. 281:301–315.
22. Barnes HA (1989) Shear-thickening (dilatancy) in suspensions of non aggregating solid particles dispersed in newtonian liquids. Journal of Rheology 33:329–366.
23. Brown E, et al. (2011) Shear thickening and jamming in densely packed suspensions of different particle shapes. Physical Review E 84:1–11.
24. Bitbol M (1986) Red blood cell orientation in orbit C= 0. Biophys. J. 49:1055–1068.
25. Yao W, et al. (2001) Low viscosity ektacytometry and its validation tested by flow chamber. J. Biomech. 34:1501–1509.
26. Keller SR, Skalak R (1982) Motion of a tank-treading ellipsoidal particle in a shear flow. J. Fluid Mech. 120:27–47.
27. Dupire J, Abkarian M, Viallat A (2015) A simple model to understand the effect of membrane shear elasticity and stress-free shape on the motion of red blood cells in shear flow. Soft Matter.
28. Dupont C, Salsac AV, Barthès-Biesel D (2013) Off-plane motion of a prolate capsule in shear flow. J. Fluid Mech. 725:180–198.
29. Cordasco D, Bagchi P (2013) Orbital drift of capsules and red blood cells in shear flow. Phys. Fluids 25:091902.
30. Sutera SP, Mehrjardi MH (1975) Deformation and fragmentation of human red blood cells in turbulent shear flow. Biophys. J. 15:1–10.
31. Lim GHW, Wortis M, Mukhopadhyay R (2002) Stomatocyte-discocyte-echinocyte sequence of the human red blood cell: Evidence for the bilayer-couple hypothesis from membrane mechanics. Proc. Natl. Acad. Sci. USA 99:16766–16769.
32. Forsyth AM, Wan J, Owrutsky PD, Abkarian M, Stone HA (2011) Multiscale approach to link red blood cell dynamics, shear viscosity, and ATP release. Proc. Natl. Acad. Sci. USA 108:10986–10991.
33. Fåhraeus R, Lindqvist T (1931) The viscosity of the blood in narrow capillary tubes. Am. J. Physiol. 96:562–568.
34. Gibaud E (2015) Numerical simulation of red blood cells flowing in a blood analyzer. PhD thesis, Université de Montpellier.
35. Dulinska I, Targosz M, Strojny W, Lekka M, Czuba P, Balwierz W, and Szymonski M (2006) Stiffness of normal and pathological erythrocytes studied by means of atomic force microscopy. J. Biochem. Biophys. Methods, 66:1–11.
36. Dodson III WR, Dimitrakopoulos P (2010) Tank-treading of erythrocytes in strong shear flows via a nonstiff cytoskeleton-based continuum computational modeling. Biophys. J., 99:2906–2916.
37. Cordasco D, Yazdani A, Bagchi P (2014) Comparison of erythrocyte dynamics in shear flow under different stress-free configurations. Phys. Fluids, 26(041902).
38. Evans EA, Fung YC (1972) Improved measurements of the erythrocyte geometry. Microvasc. Res., 4:335–347.
39. Plimpton S (1995) Fast Parallel Algorithms for Short-range Molecular-Dynamics. J. Comp. Phys., 117:1–19.
40. Español P, Revenga M (2003) Smoothed dissipative particle dynamics. Phys. Rev. E, 67:026705.
41. Groot RD, Warren PB (1997) Dissipative particle dynamics: Bridging the gap between atomistic and mesoscopic simulation. J. Chem. Phys., 107:4423.

42. Fedosov DA, Peltomaeki M, Gompper G (2014) Deformation and dynamics of red blood cells in Flow through cylindrical microchannels. Soft Matter, 10:4258–4267.

Supporting Information

1 Materials and Methods

1.1 Sample preparation

Fresh venous-blood samples were obtained from healthy consenting donors, thanks to the agreement with a local blood bank to use blood (EFS, Montpellier) and its components for non-therapeutic purposes. The samples, whose volume ranged between 420 and 500 ml, were stored in PVC-DEHP transfusion bags produced by Macopharma (MSE Systems). Such bags are provided with 66.5 ml of CPDA-1 anticoagulant (pH=5.6), whose composition is: Sodium citrate dihydrate 26.3 g/l, Citric acid monohydrate 3.27 g /l, Monobasic Sodium Phosphate dihydrate 2.51 g/l, Dextrose monohydrate 25.5 g/l. The suspensions were then centrifuged at 1000 x g for 20 min and the buffy coat was removed. RBC dispersions were diluted in PBS and the procedure of centrifugation/removal was repeated twice to obtain washed RBCs. Afterwards, cells were re-suspended in their native plasma treated with anticoagulant or in solutions of PBS supplemented with BSA (1 mg of BSA per 1 ml PBS) and the hematocrit was adjusted by using graduated and narrow test-tubes. Samples were kept at 25°C throughout all the preparation.

Dilute suspensions ($Ht = 1\%$) of fluorescent HRBCs for confocal observation were prepared by using a PKH26 Red Fluorescent Cell Linker (Sigma-Aldrich). HRBCs were labeled following standard protocol of the provider.

2,000 kDa Dextran (Leuconostoc spp., Sigma-Aldrich) solutions were prepared in PBS with a concentration of 2% (wt/wt), 4% (wt/wt), and 9% (wt/wt). Dissolution was obtained at room temperature by overnight gentle stirring. All dextran/PBS solutions showed a nearly Newtonian behavior with a constant viscosity equal to 3.4, 10.2 and 38.8 mPa.s respectively for dextran concentrations of 2% (wt/wt), 4% (wt/wt), and 9% (wt/wt). We used a very high molecular weight dextran in order not to change the osmolarity of the buffer suspension when it has been added to make the suspending medium more viscous. All dispersions containing RBCs and all suspending solutions used in our experiments have a pH ranging between 7.0 and 7.2 for WB and 7.4 for both PBS/BSA and PBS/dextran solutions. Osmolarities of our buffers were measured to be 285 mOsm on average. The samples were stored in a refrigerator at 4°C and they were used within the time frame between 3 hours and 5 days after the blood draw. The healthy state of the cells have been checked by looking at the amount of echinocytes before each experiments. Blood samples and realized experiments are summarized in Table S1.

1.2 Rheology and microfluidics

Rheology experiments were performed in a cone-plate stress-imposed rheometer (AR 2000 - TA Instrument). The temperature was kept constant at 37°C by a

Table S1: Summary of samples used for the experimental investigations. Letters in the first column indicate different patients, while symbols indicate samples used for rheological (x) and microfluidic (o) measurements. Suspension conditions are indicated as: plasma (WB) and saline solution (PBS/BSA). Dispersions with hardened cells at rest are indicated as HDisco and obtained at high shear rates as HLobe. Experiments realized in dextran solutions are marked as (dxt).

Donor	WB	PBS/BSA	HDisco	HLobe	dxt
A	x	x			
B	x	x	x		
C	x	x			
D			x		
E				x	
F		x		x	
G				x	
H					x
I		o			ox
J		o			ox
K		o			ox
L		ox			
M		o			

Peltier temperature controller. Data were analyzed by the Rheology Advantage Data Analysis software. In the first type of experiments, diluted suspensions of RBCs (Ht=1%) in a PBS/BSA solution were hardened in flow by adding a 70% wt/wt solution of glutaraldehyde prepared in PBS solution (Sigma-Aldrich) and glutaraldehyde concentration was adjusted to 9%. 300 μl of the resulting sample was added by capillarity to 700 μl of the RBC dispersion during shearing to reach a final glutaraldehyde concentration of almost 3%. Such an amount of glutaraldehyde produces a very rapid, strong and permanent solidification. Indeed, recent AFM indentation measurements [35] performed on glutaraldehyde-treated RBCs have yielded a Young's modulus E in the range 10-100 kPa. Therefore, for the maximum shear stress σ of 6 Pa reached in our experiments, the typical strain of hardened RBCs, σ/E, is expected to be within 0.05-0.005%. This means that HRBCs can be considered as rigid objects in all our experiments. The same protocol was used to harden samples at higher hematocrits. Both shearing and hardening were carried out within 2 min. Samples were then collected, washed, and suspended in PBS solution for microscopic examination.

Images of stiffened cells were acquired with an inverted microscope (Olympus IX71 60x objective) equipped with a digital camera (Sony XCD-X710). Acquired data were analyzed in Matlab (Mathworks, version 2011a): the minimum number of cells counted and classified for each $\dot{\gamma}$ in Fig. 1B of the main manuscript and for each Ht in Fig. 3A was equal to 550 and 450, respectively. Microflow observations were realized at 25°C in glass round capillaries with a diameter of 50 μm. Flow rates were adjusted by a OB1 Pressure Controller

(ElveFlow) operating up to 2 bar. Images were acquired at a high magnification (60x and 100x objectives) on a Nikon inverted microscope equipped with a high-speed camera Phantom Miro M320S (Vision Research) and subsequently analyzed by a custom image analysis software (ImageJ).

1.3 Numerical simulations

Two different in-house softwares were used for numerical simulations. The first one, YALES2BIO [19, 34], is a finite-volume parallel solver for the incompressible Navier-Stokes equations on unstructured meshes. Fluid-structure coupling was implemented using an immersed boundary method adapted to unstructured grids [19]. RBCs were modeled as viscous drops enclosed by membranes resisting shear, bending, and area dilation. In the SDPD simulations, the smoothed dissipative particle dynamics method [21], a mesoscale hydrodynamic particle-based approach, represents fluid flow, while a RBC membrane was modeled as a triangulated network of springs [20], whose vertices are coupled to the fluid via frictional forces. The network assumes fixed connectivity and includes the spring's elastic energy, bending energy, and area and volume conservation constraints [20]. Further details about the numerical methods and setups are given below.

1.3.1 YALES2BIO simulations

YALES2BIO (`http://www.math.univ-montp2.fr/~yales2bio/`) is a finite volume parallel solver for the incompressible Navier-Stokes equations on unstructured meshes. Fluid-structure coupling is accounted for by an immersed boundary method adapted to structured and unstructured grids [19], thoroughly validated in 2D and 3D [19, 34]. Red blood cells are model as viscous fluid drops enclosed by membranes resisting bending, shear, and area dilation. The Helfrich model with spontaneous curvature represents resistance to bending via the curvature energy $\mathcal{E}_b$:

$$\mathcal{E}_b = \frac{\kappa_b}{2}\int_S (2H - c_0)^2 dS, \tag{1}$$

with S the membrane surface, κ_b the bending modulus, H the mean curvature and c_0 the spontaneous curvature.

In-plane elastic resistance due to the cytoskeleton is modeled using the Skalak model:

$$W_{SK} = \frac{G_s}{4}[(\lambda_1^2 + \lambda_2^2 - 2)^2 + 2(\lambda_1^2 + \lambda_2^2 - \lambda_1^2\lambda_2^2 - 1)] + \frac{C\,G_s}{4}(\lambda_1^2\lambda_2^2 - 1)^2, \tag{2}$$

with λ_1 and λ_2 the in-plane principal values of strain, G_s the shear modulus and C a parameter representing the ratio of the area dilatation modulus to the shear modulus. As the model is used for the cytoskeleton only, C should be of the order of unity. We use $C = 0.5$ (see Ref. [36] for discussion).

The resistance to area dilation of the lipid bilayer is accounted by a global area resistance. This approach has the advantage of relaxing the well known

stiffness of the Skalak model [36], which is critical at the high shear rates considered.

Computations of the dynamics of isolated red blood cells in simple shear flow are performed in a cubic domain of edge 21 μm, delimited by a pair of sliding walls with opposite velocities imposing a shear rate $\dot{\gamma}$. Periodic boundary conditions are imposed in the other two directions. The fluid domain is discretized by a Cartesian grid of 60^3 elements, with a resolution of 0.35 μm. The same setup was already used to study tank-treading, and validated against experimental data [34]. The red blood cell is initially deposited into the undisturbed shear flow and computations are performed over 800 characteristic time units (in $1/\dot{\gamma}$) to guarantee that the dynamics reported is stable.

We used the same characteristics for the cell as Cordasco *et al.* [37]. The initial RBC shape is pre-stressed since it is transformed from an unstressed ellipsoid of volume ratio 0.997 and area 134.1 μm^2 to a discocyte having the same area and a volume of 94.1 μm^3. A positive spontaneous curvature of $c_0 = 1.41$ μm^{-1} is imposed. After a transient phase, the RBC stabilizes to an equilibrium shape very close to the parametric shape by Evans & Fung [38]. The initial shape is thus similar to the parametric biconcave shape of Evans & Fung [38], but the stress-free shape is the ellipsoid of volume ratio 0.997. As in Cordasco *et al.* [37], the bending modulus is equal to $\kappa_b = 6.0 \times 10^{-19}$ J. The Reynolds number is 0.1 in all the simulations, and the viscosity ratio is 5.0. The shear modulus is $G_s = 2.5$ $\mu\text{N.m}^{-1}$ and the local area modulus is twice as large, as $C = 0.5$ [36]. A large global area coefficient (approximately $1000\,G_s$) is imposed to conserve globally the area of the cell; variations of the membrane area always remain smaller than 0.5 %.

1.3.2 SDPD simulations

The other software we used is based on the code *LAMMPS* [39], which has been modified by our group. We have implemented SDPD, a particle-based hydrodynamics method [40], where each particle represents a microscale fluid volume. Particles in SDPD interact through pairwise conservative, dissipative, and random forces. A particle density of $12/\left(\mu m\right)^3$ was used, corresponding to a resolution of $0.54\mu m$ (the diameter of a sphere having the average volume of a solvent particle). To model fluid-structure interactions, we employed friction forces in the DPD method [41] in order to couple fluid flow and the motion of RBC membranes. The used version of SDPD conserves angular momentum [21], which is crucial for simulations with fluids having different viscosities.

The RBC is modeled as an impenetrable membrane enclosing an inner fluid. We have used bounce-back reflections at a membrane to prevent fluid particles to cross the membrane both from inside and outside [20]. The membrane was made up of 3000 vertices connected with springs. The model has featured stretching, bending and compression resistance. Governing potentials, numerical implementation, and parameter values are identical to those in Ref. [42], except where noted in the text. Local and global area, and volume conservation are modeled by penalty-like potentials. Bending energy has followed Eq. (1)

and the bending rigidity is related to thermal energy as $\kappa_b = 70 k_B T$.

An attractive worm-like-chain model, combined with a repulsive power function, imposes a spring force between two adjacent vertices:

$$\begin{aligned} U_{\text{bond}} &= U_{\text{wlc}} + U_{\text{pow}} \\ U_{\text{wlc}} &= k_B T \frac{l_m}{4p} \frac{3x^2 - 2x^3}{1 - x} \\ U_{\text{pow}}(l_i) &= \begin{cases} \frac{k_p}{(m-1) l_i^{m-1}} & \text{for } \; m > 0, m \neq 1 \\ -k_p \log(l_i) & \text{for } \; m = 1 \end{cases} \end{aligned} \tag{3}$$

where $x = l/l_m \in (0, 1)$, l is the spring length, l_m is the maximum spring extension, p is the persistence length, $k_B T$ is the energy per unit mass, k_p is the force coefficient, and m is an exponent. Young's modulus of RBC membrane was set to $18.9 \cdot 10^{-6} \frac{N}{m}$. As in YALES2BIO simulations, the RBC membrane is pre-stressed. Starting from a stress-free spheroid of volume ratio 0.96 and area 133.2 μm^2, its volume is reduced by deflation to obtain a discocyte with the same area and a volume of 92.6 μm^3.

Simulations of the dynamics of isolated RBCs in simple shear flow are performed in a domain of 30 μm $\times$ 20 μm $\times$ 30 μm, confined by a pair of rigid, sliding walls with opposite velocities imposing a shear rate of $\dot{\gamma}$. The walls are modeled by a collection of frozen SDPD particles whose structure and density match those of the suspending fluid. Periodic boundary conditions are imposed in the flow and the vorticity directions. The RBC is initially placed into an undisturbed shear flow and simulations are performed over 400 characteristic time units (in $1/\dot{\gamma}$).

For an easy comparison with other studies, we have employed the following dimensionless quantities:

- Reynolds number $Re = \frac{n \dot{\gamma} D_r^2}{\eta} = 0.3$. n is the number density, $\dot{\gamma}$ is the shear rate, D_r is the effective diameter of a RBC, and η is the external fluid viscosity.
- $\lambda = \frac{\eta_i}{\eta_o}$ is the viscosity contrast between cytosol and external plasma. Here, $\lambda = 5$.
- $\dot{\gamma}^* = \dot{\gamma} \cdot \tau$ is the dimensionless shear rate. τ is the RBC's relaxation time defined as $\tau = \frac{\eta D_r^3}{\kappa_r}$.

2 Supplementary Figures

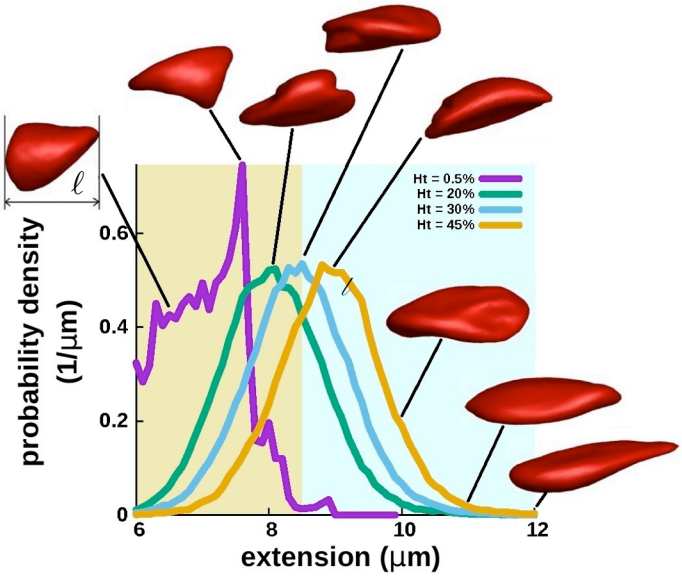

Figure S1: Distributions of RBC extension for different Ht values measured in SDPD simulations. Extension is defined as the maximum instantaneous cell length l in the flow direction, as depicted in the first inset. Distributions include data from multiple RBCs in a suspension and are averaged over many time instances. Insets illustrate typical shapes for different values of l. The two extension regions marked by light yellow and light blue colors schematically depict l ranges where polylobed shapes and creased discocytes are observed.

3 Supplementary video files

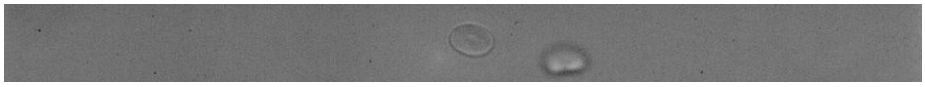

Movie S1: Folded stomatocyte with a vacillating-breathing motion in flow at $\dot{\gamma} = 500\ \mathrm{s}^{-1}$. Video was initially acquired with a high speed camera at 3500 fps in a round glass capillary with a diameter of 50 μm and is displayed here at the frame rate of 7 fps.

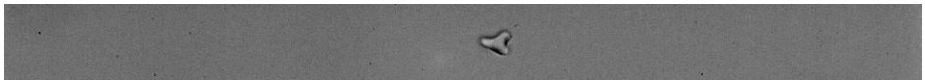

Movie S2: Side view of a trilobe RBC rotating in flow at $\dot{\gamma} = 800\ \mathrm{s}^{-1}$. Video was initially acquired with a high speed camera at 4000 fps in a round glass capillary with a diameter of 50 μm and is displayed here at the frame rate of 7 fps.

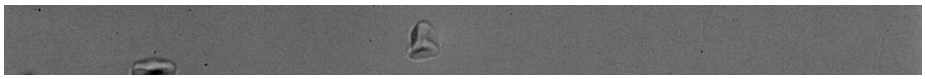

Movie S3: Hexalobe rotating in flow at $\dot{\gamma} = 850\ \mathrm{s}^{-1}$. Video was initially acquired with a high speed camera at 5000 fps in a round glass capillary with a diameter of 50 μm and is displayed here at the frame rate of 7 fps.

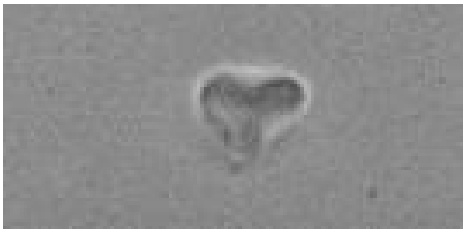

Movie S4: Relaxation of a hexalobe RBC after stopping the flow in a round glass capillary with a diameter of 50 μm . Video was initially acquired with a high speed camera at 1500 fps and is displayed here at the frame rate of 100 fps.

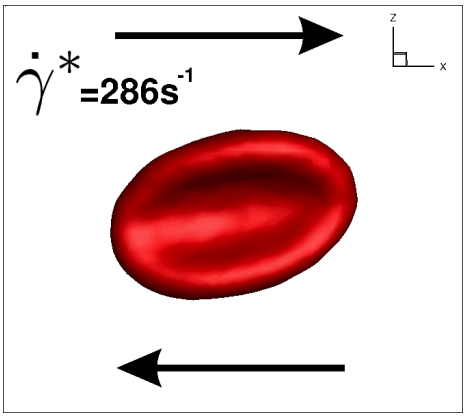

Movie S5: Folded stomatocyte showing dynamics from tumbling to rolling in flow at $\dot{\gamma} = 286s^{-1}$. SDPD simulation video of a RBC being sheared in a slit of $30\mu m$ height and periodic boundary conditions in both flow and vorticity directions. The shear profile is linear.

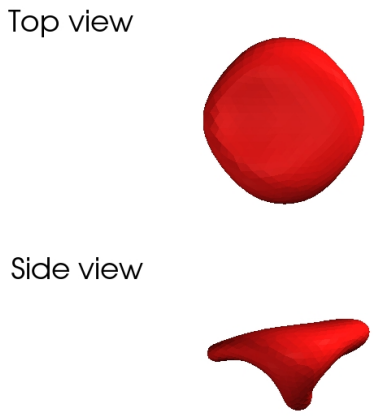

Movie S6: Top and side views of a trilobe RBC rotating in flow at $\dot{\gamma} = 1000$ s^{-1} obtained by numerical simulations using YALES2BIO. Video was generated from solutions stored at 2000 fps in pure shear flow and is displayed at the frame rate of 16 fps.

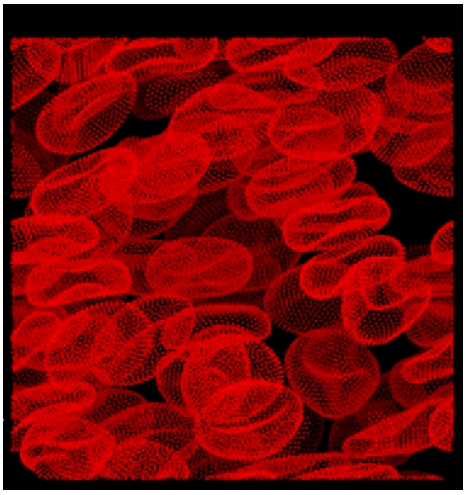

Movie S7: Concentrated suspension of RBCs ($Ht = 20\%$ and $\dot{\gamma} = 1000s^{-1}$). SDPD simulation video of RBCs being sheared under periodic boundary conditions in all directions (Lees-Edwards boundary conditions). We observe many polylobed/creased RBCs. The shear profile is linear.

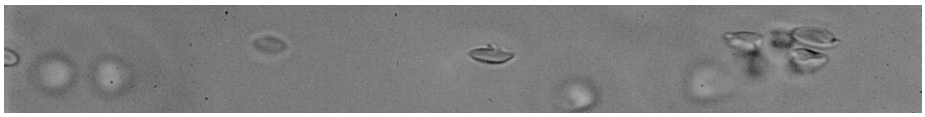

Movie S8: Polylobed RBCs rotating in flow in a PBS/BSA solution with dextran (2% wt/wt). The cells are subjected to a local shear stress of $\tau \approx 6$ Pa. Video was initially acquired with a high speed camera at 3500 fps and is displayed here at the frame rate of 5 fps.

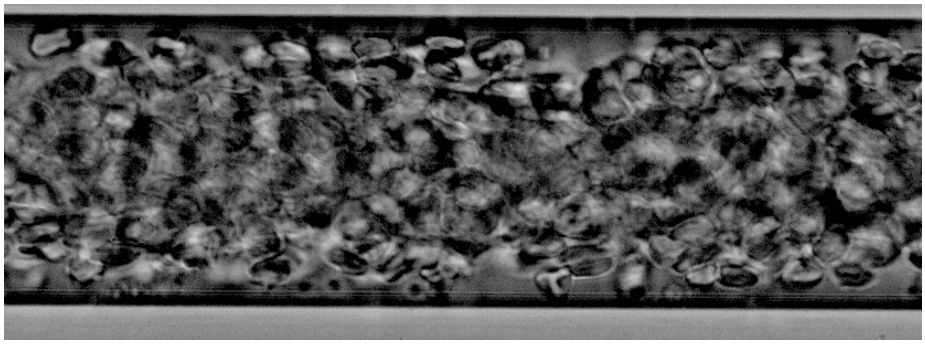

Movie S9: Concentrated suspension of RBCs ($Ht \approx 15\%$) in PBS/BSA solution flowing in a round glass capillary with a diameter of 50 μm. A large number of polylobed/creased RBCs is observed in proximity of channel walls (wall shear rate is $\dot{\gamma}_{wall} = 850$ s^{-1}). Video was initially acquired with a high speed camera at 3000 fps and is displayed here at the frame rate of 25 fps.